Heliyon 9 (2023) e13236

Contents lists available at ScienceDirect

Heliyon

journal homepage: www.cell.com/heliyon

Research article

Tension force causes cell cycle arrest at G2/M phase in osteocyte-like cell line MLO-Y4

Natsuo Shimizu [a,b], Kyoko Fujiwara [c,d,*], Kotoe Mayahara [a,e], Mitsuru Motoyoshi [a,e], Tomihisa Takahashi [c,d]

[a] Department of Orthodontics, Nihon University School of Dentistry, 1-8-3 Kanda-Surugadai, Chiyoda-ku, Tokyo, 101-8310, Japan
[b] Division of Applied Oral Science, Nihon University Graduate School of Dentistry, 1-8-3 Kanda-Surugadai, Chiyoda-ku, Tokyo, 101-8310, Japan
[c] Department of Anatomy, Nihon University School of Dentistry, 1-8-3 Kanda-Surugadai, Chiyoda-ku, Tokyo, 101-8310, Japan
[d] Division of Functional Morphology, Dental Research Center, Nihon University School of Dentistry, 1-8-3 Kanda-Surugadai, Chiyoda-ku, Tokyo, 101-8310, Japan
[e] Division of Clinical Research, Dental Research Centre, Nihon University School of Dentistry, 1-8-3 Kanda-Surugadai, Chiyoda-ku, Tokyo, 101-8310, Japan

ARTICLE INFO

Keywords:
Osteocyte
Mechanical stress
Tension force
Cell cycle arrest
Oxidative stress

ABSTRACT

Bone remodelling is the process of bone resorption and formation, necessary to maintain bone structure or for adaptation to new conditions. Mechanical loadings, such as exercise, weight bearing and orthodontic force, play important roles in bone remodelling. During the remodelling process, osteocytes play crucial roles as mechanosensors to regulate osteoblasts and osteoclasts. However, the precise molecular mechanisms by which the mechanical stimuli affect the function of osteocytes remain unclear. In the present study, we analysed viability, cell cycle distribution and gene expression pattern of murine osteocyte-like MLO-Y4 cells exposed to tension force (TF). Cells were subjected to TF with 18% elongation at 6 cycles/min for 24 h using Flexcer Strain Unit (FX-3000). We found that TF stimulation induced cell cycle arrest at G2/M phase but not cell death in MLO-Y4 cells. Differentially expressed genes (DEGs) between TF-stimulated and unstimulated cells were identified by microarray analysis, and a marked increase in glutathione-S-transferase α (GSTA) family gene expression was observed in TF-stimulated cells. Enrichment analysis for the DEGs revealed that Gene Ontology (GO) terms and Kyoto Encyclopedia Genes and Genomes (KEGG) pathways related to the stress response were significantly enriched among the upregulated genes following TF. Consistent with these results, the production of reactive oxygen species (ROS) was elevated in TF-stimulated cells. Activation of the tumour suppressor p53, and upregulation of its downstream target GADD45A, were also observed in the stimulated cells. As GADD45A has been implicated in the promotion of G2/M cell cycle arrest, these observations may suggest that TF stress leads to G2/M arrest at least in part in a p53-dependent manner.

1. Introduction

Bone remodelling is the process of bone resorption and formation, which is necessary for maintenance of bone structure and

* Corresponding author. Department of Anatomy, Nihon University School of Dentistry, 1-8-3 Kanda-Surugadai, Chiyoda-ku, Tokyo 101-8310, Japan.
E-mail address: fujiwara.kyoko@nihon-u.ac.jp (K. Fujiwara).

https://doi.org/10.1016/j.heliyon.2023.e13236
Received 16 September 2022; Received in revised form 12 January 2023; Accepted 23 January 2023
Available online 24 January 2023

adaptation to new conditions [1]. Mechanical loading plays important roles in bone remodelling. For example, orthodontic force induces bone resorption on the compression side of alveolar bone and bone formation on the tension side, resulting in tooth movement [2,3]. Osteocytes have been known to play important roles including recruitment and activation of osteoblasts and osteoclasts in bone remodelling processes [4]. Osteocytes, which are embedded in the bone lacunae, comprise more than 90% of the cellular components of the mature bone [5]. Previous studies revealed that osteocytes are the main mechanosensory cells in bone, translating mechanical strain into regulatory signals in osteoblasts and osteoclasts [6,7,8,9].

Osteocytes located in the bone tissues are exposed to various forces, including gravity, fluid shear stress (FSS), compressive and tension stresses [10]. Among them, many of studies have focused on FSS, which is generated from the interstitial fluid flow in the lacuno-canalicular system (LCS) [11]. Cultured osteocytes were reported previously to show increases in intracellular Ca^{2+} level [12], ATP release [13] and production of prostaglandin E2 [13] and nitric oxide (NO) [14] in response to FSS, which were suggested to play roles in the propagation of mechanical stimuli to neighbouring osteocytes [5] and also to affect the function of both osteoblasts and osteoclasts [15].

In addition to FSS, other types of mechanical stress, such as compressive and tension stresses, influence gene expression pattern and/or the secretion of bioactive factors by osteocytes, thereby affecting the function of the surrounding cells including osteoblasts, osteoclasts and periodontal ligament (PDL) cells. For example, it has been shown that compression force suppresses, while tension force (TF) induces WNT1 expression in MLO-Y4 murine osteocyte-like cells. Intriguingly, sclerostin secreted by MLO-Y4 cells attenuated the induction of WNT1 mRNA in PDL cells [16]. It has also been reported that TF promotes autophagy in osteocytes both *in vitro* and *in vivo*, and autophagy was shown to induce secretion of the osteogenic cytokine, fibroblast growth factor 23 (FGF23), resulting in enhancement of osteoblast viability [17]. Using a 3D compression culture model, Zarka et al. demonstrated that mechanical stress promoted nuclear translocation of YAP/TAZ and induced expression of their target genes, such as M-csf and Cxcl1 in MLO-Y4 cells [18]. Recent studies identified the microRNAs (miRs) secreted from osteocytes following exposure to tension stress, and miR-29b-3p and miR181b-5p were shown to be involved in the negative regulation of osteoblast differentiation [19] and PDL stem cell proliferation [20], respectively.

Although these findings provide some insight into how osteocytes can regulate the function of the cells involved in bone homeostasis and bone remodelling, it remains elusive whether mechanical stress affects the viability and cellular function of osteocytes. FSS promotes survival of osteocytes through the inhibition of cell death, which is mediated by nitric oxide [14]. Alternatively, Zhang et al. reported that FSS increases the viability of MLO-Y4 cells through the induction of autophagy and ATP release [21]. In contrast, Yu et al. showed that FSS promoted cell death of osteocytes by plasma membrane disruption (PMD) [22]. However, the effects of tension and compression stresses on the function of osteocytes are still unclear.

In the present study, MLO-Y4 murine osteocyte-like cells were exposed to TF and their reactions were examined partly based on gene expression profiling. We found that TF stimulation arrested the cell cycle at G2/M in MLO-Y4 cells, and the gene expression profile showed that the stimulation induced stress response genes. Consistent with this observation, production of reactive oxygen species (ROS) was increased in response to TF stimulation.

2. Materials and methods

2.1. Cells and culture conditions

Murine osteocyte-like cells, MLO-Y4, were kindly provided by Dr. Yuko Takagaki (Kanagawa Dental University, Kanagawa, Japan). Cells were cultured in MEM-α medium (Fujifilm Wako Chemicals, Kanagawa, Japan) supplemented with 5% heat-inactivated foetal bovine serum (FBS; Nichirei Bioscience, Tokyo, Japan), 5% heat-inactivated calf serum (CS; Sigma-Aldrich, St. Louis, MO, USA), 100 IU/ml of penicillin (Thermo Fisher Scientific, Waltham, MA, USA) and 100 μg/ml of streptomycin (Thermo Fisher Scientific). Cells were maintained at 37 °C in an incubator under an atmosphere of 95% air and 5% CO_2.

2.2. Mechanical loading

MLO-Y4 cells were seeded into 6-well flexible-bottom plates (Flexcell International Corp., Burlington, NC, USA) at 4×10^4 cells/well and cultured for 24 h. Cells were stimulated with tension force (TF) using a Flexcell Strain Unit (FX-3000; Flexcell International Corp.) with 18% elongation at 6 cycles/min. Control cells were seeded and cultured under the same conditions without TF.

2.3. Analysis of cell viability and cell cycle distribution

Cell viability was measured by WST8 assay. Briefly, cells were stimulated with or without TF, and then culture medium was replaced with fresh medium containing Cell Count Reagent CF (Nacalai Tesque, Kyoto, Japan). After an additional 4-h incubation without TF, 100 μl aliquots of supernatant were dispensed into 96-well plates, followed by measurement of the absorbance at 450 nm using plate reader (Spectra Max ABS plus; Molecular Devices, San Jose, CA, USA).

For cell cycle analysis, a mixture of floating and attached cells was collected from the cultures stimulated with or without TF, washed in PBS and then fixed in 70% ice-cold ethanol overnight. After washing in PBS, cells were incubated in PBS containing 0.1% FBS, 25 μg/ml of propidium iodide and 200 μg/ml of RNase A for 15 min at room temperature for the analysis by FACS Gallios (Beckman Coulter, Brea, CA, USA).

2.4. Microarray

Cells were stimulated with or without TF as described above, and total RNA was extracted from the cells using RNeasy mini kits (Qiagen, Valencia, CA, USA) according to the manufacturer's instructions. All of the samples were processed for global gene expression analysis using (Clariom S Assay; Thermo Fisher Scientific). The obtained expression array feature intensity files (CEL files) were analysed using Transcriptome Analysis Console (TAC) software ver. 4.0.2 (Thermo Fisher Scientific) to identify the differentially expressed genes (DEGs) between TF-stimulated and unstimulated groups. One-way analysis of variance (ANOVA) was used to identify genes that were significantly differentially expressed ($P < 0.05$) and those with $\geq$ 2-fold changes were selected.

2.5. Bioinformatics analyses

The R package clusterProfiler ver. 4.4.1 (https://bioconductor.org/packages/release/bioc/html/clusterProfiler.html) was used to perform enrichment analysis of Gene Ontology (GO) and Kyoto Encyclopedia Genes and Genomes (KEGG) pathway for the DEGs obtained by microarray analysis. GO enrichment analysis was performed for the 3 aspects, biological process (BP), cellular component (CC) and molecular function (MF). $P < 0.05$ was used to screen for significantly enriched GO and KEGG pathways.

2.6. Quantitative real-time RT-PCR (qPCR)

Total RNA was prepared from the indicated cells using RNeasy mini kits (Qiagen) and reverse transcribed to cDNA using iScript cDNA synthesis system (Bio-Rad Laboratories, Hercules, CA, USA). Quantitative real-time RT-PCR (qPCR) was performed using SYBR Premix Ex Taq™ (Takara, Shiga, Japan) according to the manufacturer's recommendations. The primers used in this analysis are listed in Table 1. Measurements were carried out in triplicate. A mixture of cDNA generated from total RNA prepared from MLO-Y4 cells was used as a reference. A series of dilutions of cDNA mixture was prepared and used for qPCR as templates to obtain a standard curve for each gene. The expression level of β-2-microglobulin (B2M) was used as an internal reference.

2.7. Western blotting

Cells were lysed in RIPA buffer supplemented with the inhibitor cocktail for protease (Nacalai Tesque) and phosphatase (Nacalai Tesque). The lysates were passed briefly through a 1-ml syringe with a 27G needle and then protein concentration in the lysates was measured using Bio-Rad DC kits (Bio-Rad). The lysates containing 10 μg of protein were separated by 4%–12% SDS-polyacrylamide gel electrophoresis, followed by electroblotting onto Immobilon-P membranes (Millipore, Billerica, MA, USA). The membranes were blocked with Blocking-one (Nacalai Tesque) overnight at 4 °C, and incubated with anti-GSTA1/2/5 (E6, sc-398714; Santa Cruz Biotechnology, Dallas, TX, USA), anti-GAPDH (ab9485; Abcam, Cambridge, UK), anti-p53 (ab131442; Abcam), anti-phospho-53 at Ser15 (#9248; Cell Signaling Technology, Danvers, MA, USA), and anti-GADD45A (D17E8, #4632; Cell Signaling Technology) antibodies at 4 °C. After 24-h incubation, membranes were washed in Tris-buffered saline containing 0.1% Tween 20 (TBS-T), followed by incubation with the appropriate secondary antibodies conjugated with horseradish peroxidase (GE Healthcare Life Sciences, Buckinghamshire, UK) for 1 h at room temperature. The membranes were then washed extensively in TBS-T and treated with Chemi-Lumi-One Super (Nacalai Tesque) to visualise immunoreactivities using LAS4000 (Fujifilm, Tokyo, Japan). The density of protein bands was quantified using ImageJ [23], and normalized relative to GAPDH.

2.8. Measurement of the generation of ROS

Intracellular ROS levels were measured using 2′-7′dichlorofluorescin diacetate (DCFH-DA). MLO-Y4 cells were seeded into 6-well flexible bottom plates at 1×10^5 cells/well and cultured for 24 h. After washing in Hanks balanced salt solution (HBSS), cells were incubated in loading buffer containing DCFH-DA for 30 min. The cells were then washed in HBSS and stimulated with TF in fresh medium containing Hoechst 33258 nucleic acid stain for 30 min. After final washing with HBSS, cells were observed by microscopy (CKX53 with standard fluorescence set; Olympus, Tokyo, Japan). For quantification of ROS generation, micrographs of the cells were

Table 1
The list of primers used for quantitative real-time PCR.

Primer name	Sequence (5′ - 3′)
Gsta1 forward	CTGCCTTGGCAAAAGATAGGACC
Gsta1 reverse	CTTCCAGTAGGTGGATGTCCAC
Gsta2 forward	GAGCTTGATGCCAGCCTTCTGA
Gsta2 reverse	TTCTCTGGCTGCCAGGATGTAG
Gsta5 forward	TTGATGCCAGCCTTCTGACTCC
Gsta5 reverse	TTCTCTGGCTGCCAGGATGTAG
Gadd45a forward	CCTGGAGGAAGTGCTCAGCAAG
Gadd45a reverse	GTCGTCTTCGTCAGCAGCCAG
B2m forward	CTATATCCTGGCTCACACTGA
B2m reverse	GATGCTTGATCACATGTCTCGA

taken at ×100 magnification, and fluorescent signal intensity was measured by counting the number of stained cells using ImageJ. The ratio of DCFH-DA-positive cells to all cells stained with Hoechst 33258 was calculated. To obtain representative images, micrographs were taken at ×200 magnification.

2.9. Statistical analysis

All statistical analyses except bioinformatics analyses of the microarray data were performed using JMP software ver. 11.2 (SAS Institute Inc., Cary, NC, USA). Student's *t*-test was to examine the significance of differences between paired data. One-way ANOVA followed by the post hoc Tukey test was used for analyses among multiple data. Data are presented as the mean ± SD from at least three independent experiments, and $P < 0.05$ was taken to indicate statistical significance.

3. Results

3.1. TF caused cell cycle arrest at G2/M phase in osteocytes

To examine the possible effect of TF on osteocytes, MOL-Y4 cells were simulated with TF for 24 h and cell viability was measured. As shown in Fig. 1A, the viability of TF-stimulated cells was 84.7% that of unstimulated cells. There were no obvious differences in cell morphology between the stimulated and unstimulated cells. To examine whether TF-stimulated osteocytes undergo cell death and/or cell cycle arrest, cell cycle distribution was analysed by FACS. As shown in Fig. 1B and C, the proportion of cells with G2/M DNA content was 33.3% in TF-stimulated cells and 25.7% in unstimulated cells. Along with that, proportion of the cells in G0/G1 phase was as low as 40.7% in TF-stimulated cells, while it was 53.3% in unstimulated cells. In contrast, there was no obvious difference in proportion of cells with sub-G1 DNA content between TF-stimulated cells (2.8%) and unstimulated cells (2.6%). All these results shown in Fig. 1 indicated that TF caused cell cycle arrest at G2/M phase but not cell death.

3.2. Identification of genes differentially expressed between TF-stimulated and unstimulated cells

Global gene expression analysis was performed to further address the possible effect of TF on the functions of osteocytes, and gene expression profiles were compared between TF-stimulated and unstimulated cells. Among the DEGs between TF-stimulated and unstimulated cells, 365 genes exhibited more than 2-fold higher expression level ($P < 0.05$) in the stimulated cells compared to unstimulated cells. On the other hand, 499 genes showed more than 2-fold lower expression level ($P < 0.05$) in TF-stimulated cells compared to unstimulated cells. The top 10 DEGs with higher and lower expression are listed in Tables 2 and 3, respectively. Notably, glutathione-S-transferase α (GSTA) family genes such as GSTA1, GSTA2 and GSTA5 were expressed at significantly higher levels in TF-stimulated cells in comparison to unstimulated cells. The DEGs with lower expression included virus defence-related genes, such as Oas2, Oasl2 and Ifi44, or immune cell-specific genes, such as Tgtp2 (Table 3).

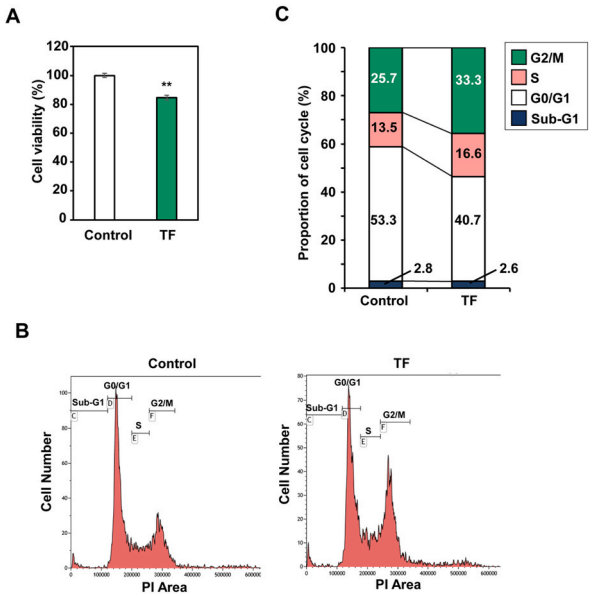

Fig. 1. TF induces G2/M cell cycle arrest of MLO-Y4 cells. (A) MLO-Y4 cells were exposed to TF for 24 h, and then cell viability was examined by WST8 assay. Data are presented as the mean ± SD of four replicates. $^{**}P < 0.01$. (B, C) For cell cycle distribution analysis, a mixture of floating and adherent cells was harvested after 24 h of TF stimulation, and then stained with propidium iodide followed by FACS analysis. The experiments were performed at least three times. Representative histograms (B) and a bar diagram showing the proportion of cell cycle distribution (C) are shown.

Table 2
Top 10 significantly up-regulated genes in TF-stimulated cells.

Gene Symbol	Description	Fold Change	FDR P-val
Gsta1	Predicted gene 3776 (Gm3776)	25.68	0.0014
Gsta2	Glutathione S-transferase, alpha 2 (Yc2)	24.5	0.0027
Procr	Protein C receptor, endothelial (Procr)	23.47	0.0027
Gm8074	Predicted gene 8074	15.92	0.0023
Gsta5	Predicted gene 10639 (Gm10639)	14.31	0.0045
Bpifc	BPI fold containing family C (Bpifc)	12.88	0.0049
Aldh3a1	Aldehyde dehydrogenase family 3, sub family A1 (Aldh3a1), transcript variant 2	11.84	0.0053
Gm21748	Predicted gene 21748 (Gm21748)	10.15	0.0066
Ovgp1	Oviductal glycoprotein 1 (Ovgp1)	9.04	0.0142
Osgin1	Oxidative stress induced growth inhibitor 1	8.53	0.0059

Table 3
Top 10 significantly down-regulated genes in TF-stimulated cells.

Gene Symbol	Description	Fold Change	FDR P-val
Tgtp2	T cell specific GTPase 2	−23.66	0.0118
Cbr2	carbonyl reductase 2	−20.7	0.0029
Stc1	stanniocalcin 1	−19.5	0.0027
Oas2	2-5 oligoadenylate synthetase 2	−19.09	0.005
Ifi44	interferon-induced protein 44	−15.87	0.0043
Gm12185	predicted gene 12185	−14.58	0.0027
Vcam1	vascular cell adhesion molecule 1	−12.5	0.0037
Oasl2	2-5 oligoadenylate synthetase-like 2	−11.45	0.0027
Cd248	CD248 antigen, endosialin	−11.26	0.0061
Col3a1	collagen, type III, alpha 1	−11.11	0.0078

3.3. GO and pathway enrichment analysis of DEGs between TF-stimulated and unstimulated cells

To estimate the functions and pathways related to the response of the cells to TF stimulation, the DEGs described above were subjected to enrichment analyses for GO terms and KEGG pathways.

With regard to the 365 genes with elevated expression in TF-stimulated cells, 612 GO terms were enriched, consisting of 542 BP, 3 CC and 70 MF. Among the 499 genes showing low expression, 733 GO terms were enriched, including 653 BP, 18 CC and 62 MF. The top 10 GO terms in each aspect according to *P*-value are shown in Fig. 2. For highly expressed genes, GO terms in the aspect of BP including response to oxidative stress, autophagy, process utilizing autophagic mechanism and response to chemical stress, were highly significantly enriched (Fig. 2A). For CC, phagophore assembly site, autophagosome and transferase complex, and transferring

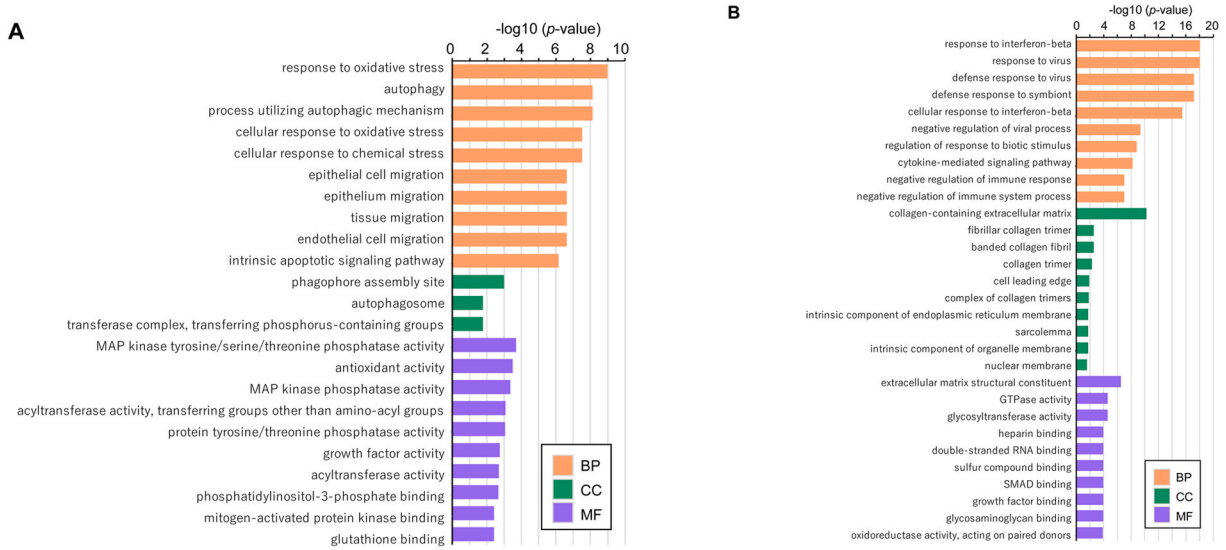

Fig. 2. GO enrichment analysis of genes differentially expressed between TF-stimulated and unstimulated cells. Among the GO terms enriched ($P < 0.05$) in upregulated genes (A) and downregulated genes (B), the top 10 terms of biological process (BP), cellular component (CC) and molecular function (MF) are listed.

phosphorus-containing groups were included. MAP kinase (MAPK) tyrosine/serine/threonine phosphatase activity, antioxidant activity, and MAPK phosphatase activity were detected as GO terms in the MF aspect. Among the genes with low expression, GO terms in BP, such as response to interferon-β, response to virus, and defence response to virus, were highly enriched (Fig. 2B). Those in CC aspect included collagen-coating extracellular matrix, fibrillar collagen trimer and banded collagen fibril. Extracellular matrix structural constituent, GTPase activity and glycosyltransferase activity were included in MF.

Based on KEGG pathway enrichment analysis, 21 and 23 pathways were enriched in 365 and 499 DEGs with high and low expression, respectively. The top 10 pathways based on *P*-value of the DEGs with high and low expression are shown in Fig. 3. Among the highly expressed genes, pathways related to MAPK signalling, hepatocellular carcinoma, FoxO signalling and glutathione metabolism were enriched (Fig. 3A). Pathways for NOD like receptor signalling, measles, COVID-19 and influenza A were enriched in the DEGs with low expression (Fig. 3B).

3.4. Strong induction of GSTA family genes by tension force

Upregulation of GSTA family genes, such as GSTA1, GSTA2 and GSTA5, in the stimulated cells was confirmed at the RNA and protein levels (Fig. 4A and B). The mRNA expression levels of GSTA1, GSTA2 and GSTA5 were 7.2, 8.6 and 8.0 times higher in TF-stimulated than unstimulated cells, respectively. The protein level was 1.8 times higher in the stimulated cells compared to unstimulated cells. Time course analysis revealed that the expression levels of GSTA mRNAs were markedly increased in a time-dependent manner (Fig. 4C). Even after 30-min TF stimulation, mRNA expression levels of GSTA1, GSTA2 and GSTA5 were 1.3, 1.2 and 1.4 times higher than those in unstimulated cells, respectively, which increased to 1.9, 2.0 and 2.5 times higher after 3-h TF stimulation.

As GSTAs are induced by oxidative stress [24], and TF stimulation in MLO-Y4 cells increased the expression of genes related to oxidative stress (Figs. 2A and 3A), intracellular ROS levels were measured. As expected, TF stimulation increased intracellular ROS levels compared to controls. In stimulated cells, the ratio of cells stained with the ROS-specific dye, DCFH-DA, was more than twice

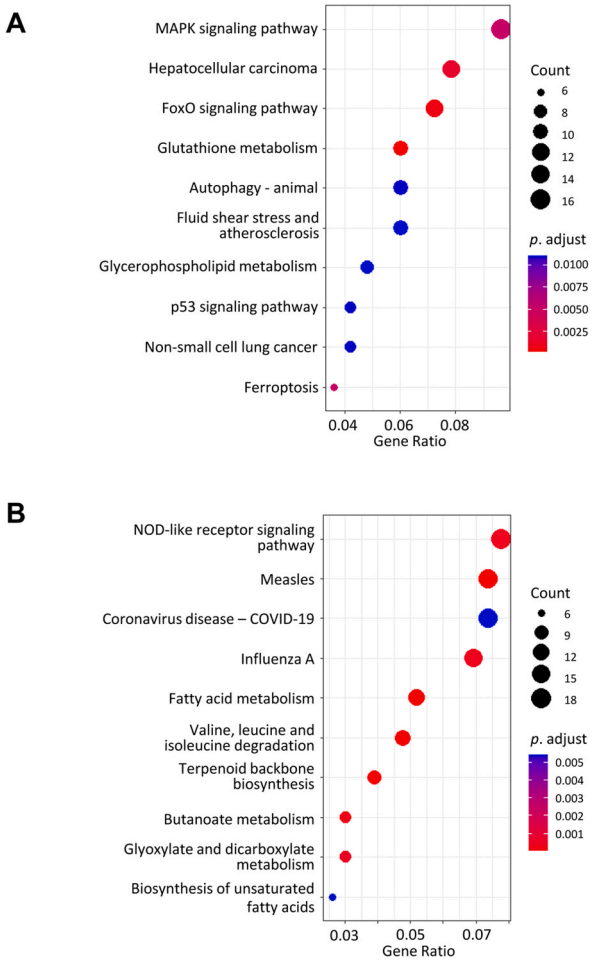

Fig. 3. Pathway enrichment analysis of genes differentially expressed between TF-stimulated and unstimulated cells. The top 10 KEGG pathways enriched ($P < 0.05$) in upregulated genes (A) and downregulated genes (B) are shown.

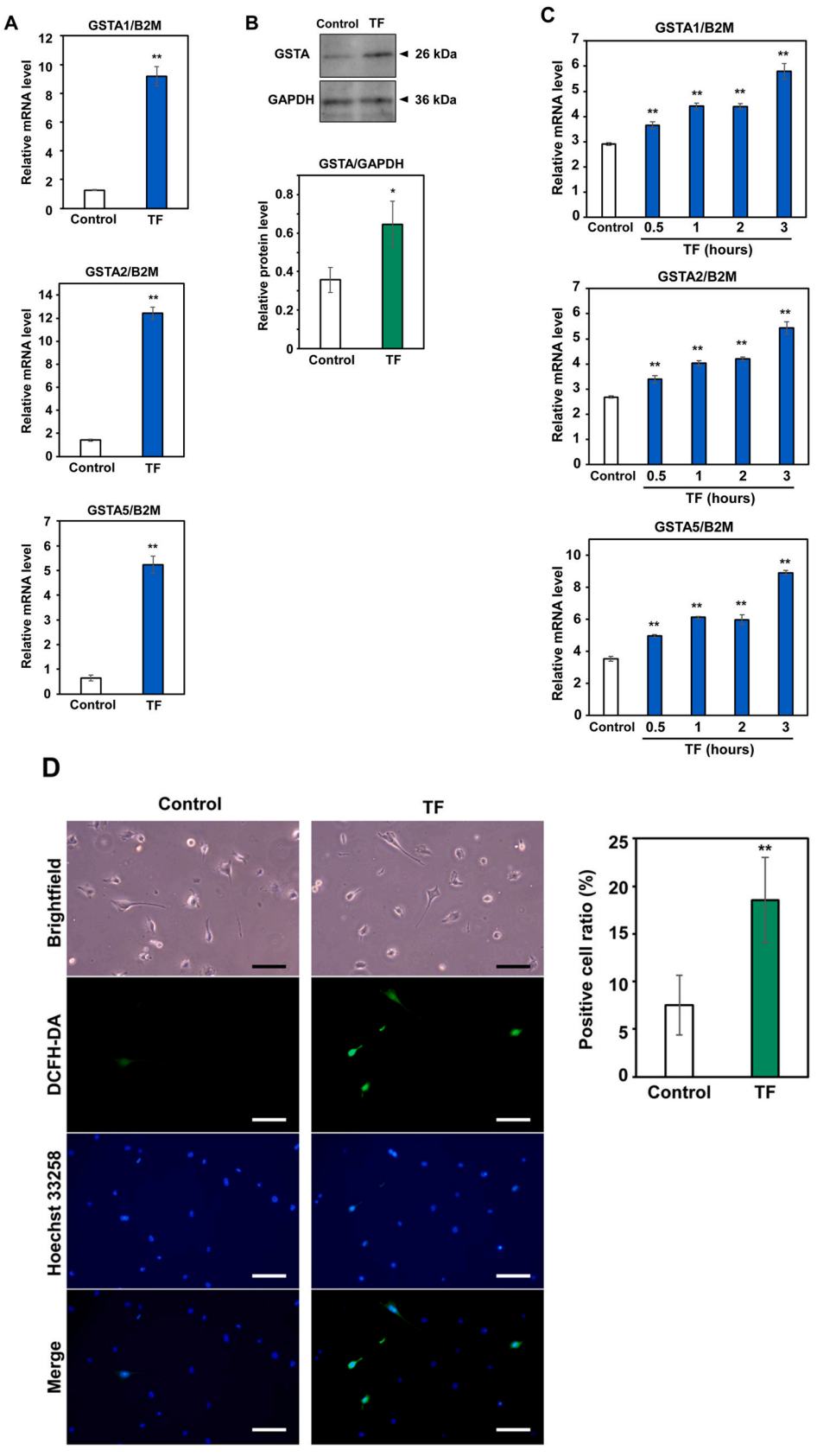

(caption on next page)

Fig. 4. GSTAs are induced in response to TF stimulation accompanied by ROS production. (A) MLO-Y4 cells were stimulated with TF for 24 h, after which total RNA was prepared and analysed for GSTA1, GSTA2 and GSTA5 expression by qPCR. Data are presented as the mean ± SD of three replicates. $^{**}P < 0.01$. (B) MLO-Y4 cells were treated in the same way as in (A) and then whole-cell lysates were prepared and analysed by Western blotting using an antibody that simultaneously recognises GSTA1, GSTA2 and GSTA5. GAPDH was used as a loading control. Representative images and quantitative plots are shown. Data are presented as the mean ± SD of three replicataes. $^{*}P < 0.05$. Full and non-adjusted images of immunoblots were shown in the supplementary material (Fig. S1). (C) MLO-Y4 cells were stimulated with TF for the indicated time, after which total RNA was extracted and analysed for GSTA1, GSTA2 and GSTA5 expression by qPCR. Data are presented as the mean ± SD of three replicataes. Statistical analyses were performed between control and each time point. $^{**}P < 0.01$ (D) MLO-Y4 cells were stimulated with TF for 30 min in the presence of Hoechst 33258 and the ROS indicator DCFH-DA. Representative images taken under a fluorescence microscope at ×200 magnification are shown (left panel). The bars indicate 100 μm. The ratio of DCFH-DA-positive cells to all cells was determined by analysing micrographs taken at ×100 magnification (right panel). Data are presented as the mean ± SD of five replicataes. $^{**}P < 0.01$.

that in unstimulated cells (Fig. 4D).

3.5. Tension force augments tumour suppressor p53

Among the genes upregulated in TF stimulated MLO-Y4 cells, several pathways related to the stress response, such as pathways for MAPK signalling, FoxO and p53 signalling, were enriched (Fig. 3A). Among them, GADD45A was commonly included. As GADD45A is known to be a direct target of p53 and has been implicated in the inhibition of cell cycle progression, we examined the levels of p53 and

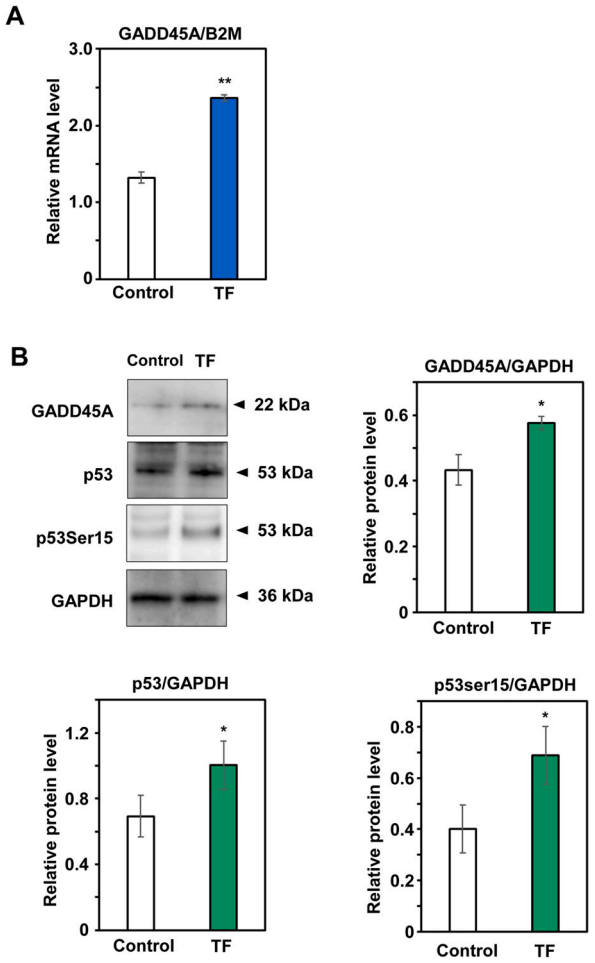

Fig. 5. TF-mediated activation of tumour suppressor p53 and induction of its target GADD45A. (A) MLO-Y4 cells were stimulated with TF for 24 h, after which total RNA was prepared and analysed for GADD45A expression by qPCR. Data are presented as the mean ± SD of three replicataes. $^{**}P < 0.01$. (B) MLO-Y4 cells were treated in the same way as in (A) and then whole-cell lysates were prepared and subjected to Western blotting to detect the protein level of GADD45A, p53 and p53 phosphorylated at Ser15 (p53Ser15). GAPDH was used as a loading control. Representative images and quantitative plots are shown. Data are presented as the mean ± SD of three replicataes. $^{*}P < 0.05$. Full and non-adjusted images of immunoblots were shown in the supplementary material (Fig. S1).

GADD45A in the presence or absence of TF stimulation. As expected, the levels of GADD45A mRNA in TF-stimulated MLO-Y4 cells were 1.8-fold higher than in unstimulated cells (Fig. 5A). Consistent with this observation, Western blotting analysis showed that TF stimulation induced 1.3 times higher GADD45A protein level compared to unstimulated cells. In addition, TF stimulation increased the protein level of p53 accompanied by its phosphorylation at Ser15 (Fig. 5B). Protein levels of p53 and phosphorylated form of it were 1.4 and 1.7 times higher in the stimulated cells than in unstimulated cells, respectively.

4. Discussion

The results of the present study showed that murine osteocyte-like MOL-Y4 cells undergo cell cycle arrest at G2/M phase in response to TF. Global gene expression analysis revealed that GSTA family genes were notably upregulated in TF-stimulated cells. Enrichment analysis for GO and KEGG pathways showed that TF stimulation induced the stress response in MLO-Y4 cells. Consistent with these results, TF stimulation caused ROS production in MLO-Y4 cells. It has been reported that mechanical stresses generates ROS through the activation of NADPH oxidase (NOX) in a variety of cells including cardiac myocytes [25], vascular endothelial cells [26] and embryonic stem cells [27]. In osteocytes, FSS activated NADPH oxidase 2 (NOX2) to produce ROS [15]. Our results showed that TF stimulation produced ROS in MLO-Y4 cells. Further studies are required to confirm whether this TF-mediated ROS production is induced through the same mechanism as that induced by FSS.

The present results showed that TF stimulation arrested the cell cycle at G2/M but did not induce cell death in MLO-Y4 cells. ROS are among the major causes of DNA damage, potentiating the p53-dependent DNA damage response [28]. Upon DNA damage, p53 is rapidly accumulated through its phosphorylation, and transactivates its downstream target genes, such as GADD45, p21cip1 and 14-3-3σ, involved in cell cycle arrest and/or induction of cell death [29]. Indeed, TF stimulation led to accumulation of p53 together with its phosphorylation at Ser15. Analysis using mutant p53 showed that phosphorylation of p53 at Ser15 prevented degradation of p53 and kept it active [30]. Notably, one of its target gene products, GADD45A, which has been implicated in the promotion of G2/M cell cycle arrest, was upregulated in TF-stimulated cells. Therefore, it is likely that cell cycle arrest at G2/M by TF stimulation may be at least in part p53-dependent. Although it is unclear why TF stimulation did not induce cell death, the observation that GO terms and pathways related to autophagy were enriched in the TF-stimulated cells suggests the possibility that TF-mediated potentiation of the autophagy pathway may prevent cell death caused by TF-induced ROS, as autophagy has a protective effect against cell death in a variety of cells [31,32].

Intriguingly, TF stimulation resulted in upregulation of GSTA family genes (Fig. 4A–C). Enrichment analysis revealed that a pathway related to glutathione metabolism was activated by TF stimulation. The expression levels of many genes in this pathway, including GSTA, GSTP, GSTM and glutamate cysteine ligase (Gclm), were upregulated by TF stimulation. As the glutathione system is crucial to reduce ROS in cells and genes involved in the glutathione system are known to be induced by ROS [33], it is likely that ROS produced by TF stimulation enhanced the expression of these glutathione enzymes. The GST superfamily belongs to the Phase II enzyme, which detoxify xenobiotics or intrinsic metabolites, including products of oxidative stress, by conjugation of them with glutathione [34]. Among the members of the superfamily, GSTAs are the most abundant GSTs expressed in the liver [35]. The specific roles of GSTAs in osteocytes and/or bone tissues have not been reported. Further studies are needed to understand why TF stimulation strongly induced the expression of GSTAs, and whether GSTAs could play specific roles in osteocytes during the stimulation.

An important limitation of this study is that an osteocyte-like cell line was used rather than primary osteocytes. Unlike MLO-Y4 cells, which are immortalized and undergo proliferation, primary osteocytes are post-mitotic cells and do not replicate. In vivo studies have demonstrated that an appropriate amount of mechanical loading suppresses osteocyte apoptosis, while overloading induces apoptosis of these cells [6,36]. The exact mechanisms underlying the death or survive of osteocytes in response to mechanical loading have not been fully elucidated. The possibility that mechanical stress induces senescence, which could inhibit apoptosis by inducing the senescent cell anti-apoptotic pathway, has been suggested [37,38]. However, this has not been verified in osteocytes. As the p53-dependent DNA damage response pathway is commonly involved in the regulation of G2/M arrest, senescence and apoptosis, clarification of the molecular mechanisms that TF stimulation induced cell cycle arrest but not cell death in MLO-Y4 cells may provide insights to understand the biphasic effect of mechanical loading on primary osteocytes. Another limitation of this study is that we focused only on the effects of TF stress on osteocyte viability. Further studies to verify whether the opposite force, i.e., compressive force could also affect cell cycle progression are needed to understand the effects of mechanical stress on osteocytes. Furthermore, this study could not corroborate that TF-produced ROS is the cause of G2/M arrest. Additional studies with modulation of ROS level using antioxidants or ROS inducers are needed to confirm the involvement of ROS in TF-induced G2/M arrest.

5. Conclusion

The results of the present study showed that TF stimulation caused cell cycle arrest at G2/M in osteocyte-like MLO-Y4 cells. Consistent with this observation, TF stimulation augmented ROS production and activated the cell cycle regulatory p53 pathway in MLO-Y4 cells.

Declarations

Author contributions statement

Natsuo Shimizu: Performed the experiments.

Kyoko Fujiwara: Conceived and designed the experiments; Performed the experiments; Analysed and interpreted the data; Contributed reagents, materials, analysis tools or data; Wrote the paper.

Kotoe Mayahara: Contributed reagents, materials, analysis tools or data.

Mitsuru Motoyoshi: Conceived and designed the experiments.

Tomihisa Takahashi: Conceived and designed the experiments; Wrote the paper.

Funding

The present study was supported in part by KAKENHI (grant number JP20K09999), the Grant from Dental Research Center, Nihon University School of Dentistry, and the Sato Fund, Nihon University School of Dentistry.

Availability of data and materials

The data used in this study are available from the corresponding author.

Declaration of interests statement

The authors declare that they have no competing interests.

Appendix A. Supplementary data

Supplementary data to this article can be found online at https://doi.org/10.1016/j.heliyon.2023.e13236.

References

[1] L.J. Raggatt, N.C. Partridge, Cellular and molecular mechanisms of bone remodeling, J. Biol. Chem. 285 (2010) 25103–25108, https://doi.org/10.1074/JBC.R109.041087.

[2] R.S. Masella, M. Meister, Current concepts in the biology of orthodontic tooth movement, Am. J. Orthod. Dentofacial Orthop. 129 (2006) 458–468, https://doi.org/10.1016/J.AJODO.2005.12.013.

[3] S. Lv, J. Li, W. Feng, H. Liu, J. Du, J. Sun, J. Cui, B. Sun, X. Han, K. Oda, N. Amizuka, X. Xu, M. Li, Expression of HMGB1 in the periodontal tissue subjected to orthodontic force application by Waldo's method in mice, J. Mol. Histol. 46 (2015) 107–114, https://doi.org/10.1007/S10735-014-9606-Z.

[4] J. Klein-Nulend, A.D. Bakker, R.G. Bacabac, A. Vatsa, S. Weinbaum, Mechanosensation and transduction in osteocytes, Bone 54 (2013) 182–190, https://doi.org/10.1016/J.BONE.2012.10.013.

[5] M. Maycas, P. Esbrit, A.R. Gortázar, Molecular mechanisms in bone mechanotransduction, Histol. Histopathol. 32 (2017) 751–760, https://doi.org/10.14670/HH-11-858.

[6] B.S. Noble, N. Peet, H.Y. Stevens, A. Brabbs, J.R. Mosley, G.C. Reilly, J. Reeve, T.M. Skerry, L.E. Lanyon, Mechanical loading: biphasic osteocyte survival and targeting of osteoclasts for bone destruction in rat cortical bone, Am. J. Physiol. Cell Physiol. 284 (2003), https://doi.org/10.1152/AJPCELL.00234.2002.

[7] L.F. Bonewald, Mechanosensation and transduction in osteocytes, BoneKEy-Osteovision 3 (2006) 7–15, https://doi.org/10.1138/20060233.

[8] L. You, S. Temiyasathit, P. Lee, C.H. Kim, P. Tummala, W. Yao, W. Kingery, A.M. Malone, R.Y. Kwon, C.R. Jacobs, Osteocytes as mechanosensors in the inhibition of bone resorption due to mechanical loading, Bone 42 (2008) 172–179, https://doi.org/10.1016/J.BONE.2007.09.047.

[9] X. Lai, C. Price, S. Modla, W.R. Thompson, J. Caplan, C.B. Kirn-Safran, L. Wang, The dependences of osteocyte network on bone compartment, age, and disease, Bone Res 3 (2015), https://doi.org/10.1038/BONERES.2015.9.

[10] Z. Wang, Y. Ishihara, T. Ishikawa, M. Hoshijima, N. Odagaki, E.E.H. Hlaing, H. Kamioka, Screening of key candidate genes and pathways for osteocytes involved in the differential response to different types of mechanical stimulation using a bioinformatics analysis, J. Bone Miner. Metabol. 37 (2019) 614–626, https://doi.org/10.1007/S00774-018-0963-7.

[11] L. Wang, S.P. Fritton, S.C. Cowin, S. Weinbaum, Fluid pressure relaxation depends upon osteonal microstructure: modeling an oscillatory bending experiment, J. Biomech. 32 (1999) 663–672, https://doi.org/10.1016/S0021-9290(99)00059-7.

[12] C.T. Hung, F.D. Allen, S.R. Pollack, C.T. Brighton, Intracellular Ca2+ stores and extracellular Ca^{2+} are required in the real-time Ca^{2+} response of bone cells experiencing fluid flow, J. Biomech. 29 (1996) 1411–1417, https://doi.org/10.1016/0021-9290(96)84536-2.

[13] D.C. Genetos, D.J. Geist, D. Liu, H.J. Donahue, R.L. Duncan, Fluid shear-induced ATP secretion mediates prostaglandin release in MC3T3-E1 osteoblasts, J. Bone Miner. Res. 20 (2005) 41–49, https://doi.org/10.1359/JBMR.041009.

[14] S.D. Tan, A.D. Bakker, C.M. Semeins, A.M. Kuijpers-Jagtman, J. Klein-Nulend, Inhibition of osteocyte apoptosis by fluid flow is mediated by nitric oxide, Biochem. Biophys. Res. Commun. 369 (2008) 1150–1154, https://doi.org/10.1016/J.BBRC.2008.03.007.

[15] J.S. Lyons, H.C. Joca, R.A. Law, K.M. Williams, J.P. Kerr, G. Shi, R.J. Khairallah, S.S. Martin, K. Konstantopoulos, C.W. Ward, J.P. Stains, Microtubules tune mechanotransduction through NOX2 and TRPV4 to decrease sclerostin abundance in osteocytes, Sci. Signal. 10 (2017), https://doi.org/10.1126/SCISIGNAL.AAN5748.

[16] E. Ei Hsu Hlaing, Y. Ishihara, N. Odagaki, Z. Wang, M. Ikegame, H. Kamioka, The expression and regulation of Wnt1 in tooth movement-initiated mechanotransduction, Am. J. Orthod. Dentofacial Orthop. 158 (2020) e151–e160, https://doi.org/10.1016/J.AJODO.2020.08.006.

[17] H. Xu, M. Xia, L. Sun, H. Wang, W.B. Zhang, Osteocytes enhance osteogenesis by autophagy-mediated FGF23 secretion under mechanical tension, Front. Cell Dev. Biol. 9 (2022), https://doi.org/10.3389/FCELL.2021.782736.

[18] M. Zarka, F. Etienne, M. Bourmaud, D. Szondi, J.M. Schwartz, K. Kampmann, C. Helary, F. Rannou, E. Haÿ, M. Cohen-Solal, Mechanical loading activates the YAP/TAZ pathway and chemokine expression in the MLO-Y4 osteocyte-like cell line, Lab. Invest. 101 (2021) 1597–1604, https://doi.org/10.1038/S41374-021-00668-5.

[19] Q. Zeng, Y. Wang, J. Gao, Z. Yan, Z. Li, X. Zou, Y. Li, J. Wang, Y. Guo, miR-29b-3p regulated osteoblast differentiation via regulating IGF-1 secretion of mechanically stimulated osteocytes, Cell. Mol. Biol. Lett. 24 (2019), https://doi.org/10.1186/S11658-019-0136-2.

[20] P.Y. Lv, P.F. Gao, G.J. Tian, Y.Y. Yang, F.F. Mo, Z.H. Wang, L. Sun, M.J. Kuang, Y.L. Wang, Osteocyte-derived exosomes induced by mechanical strain promote human periodontal ligament stem cell proliferation and osteogenic differentiation via the miR-181b-5p/PTEN/AKT signaling pathway, Stem Cell Res. Ther. 11 (2020), https://doi.org/10.1186/S13287-020-01815-3.

[21] B. Zhang, R. Hou, Z. Zou, T. Luo, Y. Zhang, L. Wang, B. Wang, Mechanically induced autophagy is associated with ATP metabolism and cellular viability in osteocytes in vitro, Redox Biol. 14 (2018) 492–498, https://doi.org/10.1016/J.REDOX.2017.10.021.
[22] K. Yu, D.P. Sellman, A. Bahraini, M.L. Hagan, A. Elsherbini, K.T. Vanpelt, P.L. Marshall, M.W. Hamrick, A. McNeil, P.L. McNeil, M.E. McGee-Lawrence, Mechanical loading disrupts osteocyte plasma membranes which initiates mechanosensation events in bone, J. Orthop. Res. 36 (2018) 653–662, https://doi.org/10.1002/JOR.23665.
[23] C.A. Schneider, W.S. Rasband, K.W. Eliceiri, NIH Image to ImageJ: 25 years of image analysis. https://doi.org/10.1038/nmeth.2089, 2012.
[24] M. Di-Luoffo, C. Brousseau, F. Bergeron, J.J. Tremblay, The transcription factor MEF2 is a Novel Regulator of Gsta Gene Class in Mouse MA-10 Leydig cells, Endocrinology 156 (2015) 4695–4706, https://doi.org/10.1210/EN.2015-1500.
[25] S.H. Woo, J.C. Kim, N. Eslenur, T.N. Trinh, L.N.H. Do, Modulations of cardiac functions and pathogenesis by reactive oxygen species and natural antioxidants, Antioxidants (Basel, Switzerland) 10 (2021), https://doi.org/10.3390/ANTIOX10050760.
[26] R.P. Brandes, J. Kreuzer, Vascular NADPH oxidases: molecular mechanisms of activation, Cardiovasc. Res. 65 (2005) 16–27, https://doi.org/10.1016/J.CARDIORES.2004.08.007.
[27] F. Sharifpanah, S. Behr, M. Wartenberg, H. Sauer, Mechanical strain stimulates vasculogenesis and expression of angiogenesis guidance molecules of embryonic stem cells through elevation of intracellular calcium, reactive oxygen species and nitric oxide generation, Biochim. Biophys. Acta 1863 (2016) 3096–3105, https://doi.org/10.1016/J.BBAMCR.2016.10.001.
[28] F.A. Mallette, G. Ferbeyre, The DNA damage signaling pathway connects oncogenic stress to cellular senescence, Cell Cycle 6 (2007) 1831–1836, https://doi.org/10.4161/CC.6.15.4516.
[29] S. Nicolai, A. Rossi, N. Di Daniele, G. Melino, M. Annicchiarico-Petruzzelli, G. Raschellà, DNA repair and aging: the impact of the p53 family, Aging (Albany. NY) 7 (2015) 1050–1065, https://doi.org/10.18632/AGING.100858.
[30] S.Y. Shieh, M. Ikeda, Y. Taya, C. Prives, DNA damage-induced phosphorylation of p53 alleviates inhibition by MDM2, Cell 91 (1997) 325–334, https://doi.org/10.1016/S0092-8674(00)80416-X.
[31] M. Kurihara, Y. Mukudai, H. Watanabe, M. Asakura, Y. Abe, A. Houri, J. Chikuda, T. Shimane, T. Shirota, Autophagy prevents osteocyte cell death under hypoxic conditions, Cells Tissues Organs 210 (2021) 326–338, https://doi.org/10.1159/000519086.
[32] S. Zhao, W. Wu, X. Lin, M. Shen, Z. Yang, S. Yu, Y. Luo, Protective effects of dexmedetomidine in vital organ injury: crucial roles of autophagy, Cell. Mol. Biol. Lett. 27 (2022), https://doi.org/10.1186/S11658-022-00335-7.
[33] M. Jaganjac, L. Milkovic, S.B. Sunjic, N. Zarkovic, The NRF2, thioredoxin, and glutathione system in tumorigenesis and anticancer therapies, Antioxidants (Basel, Switzerland) 9 (2020) 1–41, https://doi.org/10.3390/ANTIOX9111151.
[34] N. Tetlow, D. Liu, P. Board, Polymorphism of human Alpha class glutathione transferases, Pharmacogenetics 11 (2001) 609–617, https://doi.org/10.1097/00008571-200110000-00007.
[35] S.N. Silva, A.P. Azevedo, V. Teixeira, J.E. Pina, J. Rueff, J.F. Gaspar, The role of GSTA2 polymorphisms and haplotypes in breast cancer susceptibility: a case-control study in the Portuguese population, Oncol. Rep. 22 (2009) 593–598, https://doi.org/10.3892/OR_00000477.
[36] O.D. Kennedy, B.C. Herman, D.M. Laudier, R.J. Majeska, H.B. Sun, M.B. Schaffler, Activation of resorption in fatigue-loaded bone involves both apoptosis and active pro-osteoclastogenic signaling by distinct osteocyte populations, Bone 50 (2012) 1115–1122, https://doi.org/10.1016/J.BONE.2012.01.025.
[37] E.O. Wissler Gerdes, Y. Zhu, T. Tchkonia, J.L. Kirkland, Discovery, development, and future application of senolytics: theories and predictions, FEBS J. 287 (2020) 2418–2427, https://doi.org/10.1111/FEBS.15264.
[38] V.D. Sherk, C.J. Rosen, Senescent and apoptotic osteocytes and aging: exercise to the rescue? Bone 121 (2019) 255–258, https://doi.org/10.1016/J.BONE.2019.02.006.